Chapter 3

Experimental Setup

"Everything that can be invented has been invented"

Charles H. Duell (Comissioner at the U.S. Office of Patents), 1899

The present chapter is dedicated to the description of the experimental setup used. In the following sections an outline of the vacuum system (Chapter 3.1.) in which the cluster source (Chapter 3.2) is producing the aggregates will be given. The clusters were investigated by making use of various ionization means (Chapter 3.3) and the products of the processes occurring were recorded with the detectors described in Chapter 3.4.

3.1 The Vacuum Systems

Throughout the experiments performed, due to the use of two completely different recording systems, two different vacuum systems were employed.

In the vacuum system presented in Fig. 3.1 (a) the interaction region between the cluster beam and the ionizing beam takes place in a volume confined in the cubical recipient (1).
On one side of the cube one can find the cluster source (2) attached via a water cooled valve (8). On the opposite face, the cube is connected to a 53 l/s turbo-molecular vacuum pump (of the Pfeiffer TMH 064 type) via a T-piece (3), in order to pump out the excess aggregates not ionized in the interaction region and to improve the vacuum in the system.

The role of the valve (8) is to ensure that the viton rings used between the oven recipient and the experimental chamber stay intact. It also allows for a separation of the oven chamber from the cubical recipient without breaking the vacuum in case a refill of the oven source is needed. Moreover, on the side of the valve facing the experimental chamber, a pin hole has been mounted

(ϕ = 2 mm) to narrow the cluster beam entering the experimental recipient, thus reducing the divergence of the cluster beam in the interaction region.

On the lower face of the cubical recipient a blind flange (4) on which the extraction plates of the mass spectrometer, as well as the electron detector (channeltron) with their respective electrical throughputs are attached. The upper face is connected to the housing of the time-of-flight mass spectrometer (5), where a 190 l/s turbo-molecular vacuum pump (of the Pfeiffer TMH 260 PC type) is attached (not visible in the Fig. 3.1 (a)). Thus, a background pressure of 8×10^{-7} mbar to 9×10^{-7} mbar was achieved, while the running cluster source yielded a pressure of the order of 3×10^{-6} mbar.

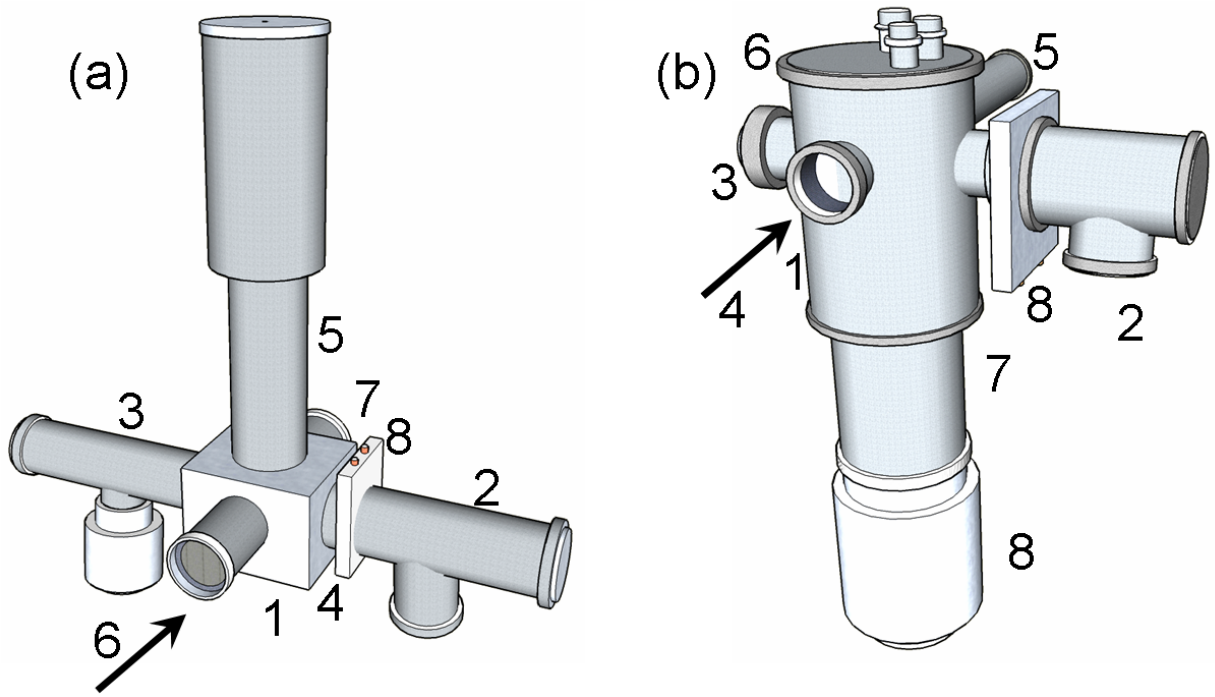

Fig. 3.1: Schematics of the two vacuum systems used

Perpendicular to the cluster beam, the cubical recipient is clamped to the radiation source (6), whereas on the opposite face a beam dump was used (7). It is important to mention that during the experiments performed at BESSY II a differential pumping stage was used to separate the experimental setup from the beam line, in order to avoid the breaking of the vacuum or the contamination of the synchrotron beam line.

The vacuum system presented in Fig. 3.1 (b) consists of a ISO-K DN 270 tubing (1), on which four lateral ports with arcs of 90° between the centers have been welded.

In a similar manner to the previous case, on one of the ports, the cluster source (2) was clamped via the water-cooled valve (8) while on the opposite port a cluster beam dump was used (3).
One of the perpendicular ports (4) to the cluster beam was connected to the differential pumping stage attached to the BESSY II beam line, while on the opposing port a beam dump (5) was constructed. This consists of a long straight tubing ended with a quartz window, with the role of minimizing the amount of stray electrons produced that would arrive at the electron detector.
The upper flange (6) serves as a support for the spectrometer, while via an ISO-K DN 270/160 reducing adapter(7), a 400 l/s magnetic bearing turbo-molecular pump (of the Pfeiffer TMH 400 MPH type) is connected (8). The typical background pressure in the vacuum system was of the order of 8×10^{-7} mbar while the experimental conditions yielded a pressure in the range of 3×10^{-6} mbar.

3.1.1 The Oven

The chalcogene clusters are produced by means of evaporation of solids in a two-stage oven. A schematics of the cluster source is presented in Fig. 3.2.

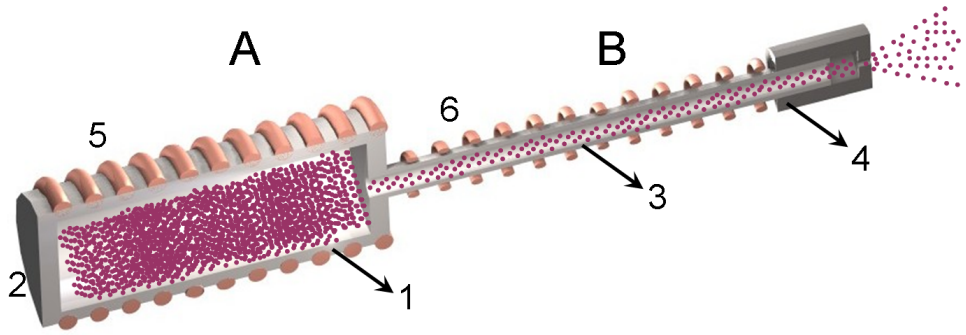

Fig. 3.2: Schematics of two staged oven cluster source

The oven source was constructed from stainless steel in order to be corrosion resistant and it consists of two separate stages, A and B.
Stage A consists of a tubing (1) with the inner diameter of 15 mm and the outer diameter of 25 mm, terminated on one side with a stainless steel cap (2). The cap is fixed with six M2 screws so that it can be easily removed in order to refill the cluster source.
Connected to stage A, a second tubing (3) of 6 mm outer diameter and 4 mm inner diameter is to be found. This, together with the stainless steel cap (4) with an opening of 2 mm terminating it, form the second stage, B, of the cluster source.

Both stages of the cluster source can be heated up via the independent resistors (5) and (6) purchased from the Thermocoax GmbH company. Heater (5) is of the SEA 20/150-10/CV 20 type and it can deliver up to 500 W at 48 V, while the heating element (6) is of the SEI 10/50-15/CV 10 type, delivering up to 100 W at 25 V. For measuring the temperature, type K thermocouples of types TKI 10/10 and TKI 20/25, respectively were used.

In stage A, the solid sample is molten, while in the B part the vapor is heated up to the desired experimental temperature.
The use of two independent heating stages of the cluster source has been chosen due to three major advantages over single stage oven sources:

(a) the temperature of the oven can be better controlled, and thus, the experimental conditions are easier adjusted to the desired parameters,

(b) by adjusting the temperature in stage A while keeping the temperature of stage B constant, one has control over the amount of sample flowing towards the experimental chamber,

(c) long operation intervals can be achieved without the need to refill, as there is no need to heat up the entire solid sample to the experimentally desired temperature, which could lead to a faster effusion of the sample in the vacuum chamber and an emptying of the oven.

3.2 Ionization Means

As the purpose of the present work was to investigate the ionization and the fragmentation of chalcogene clusters, the following sections will present an overview of the ionization means used.

During the tests performed in the laboratory, mainly a microwave-driven He (I) discharge light source has been used. The He (I) discharge lamp provides photons with $h\nu$ = 21.22 eV, which is situated above the ionization energy of sulfur and selenium aggregates, these lying around 9 eV. This ionization light source will be described in Chapter 3.2.1.

The fragmentation of sulfur clusters after inner-shell excitation has been previously investigated [11]. The photon-induced inner-shell excitation starts with a well-defined site within the cluster which relaxes via an Auger process leading to holes in the valence shell. This is then followed by fission leading eventually to the formation of singly charged products. By contrast, the ionization by *Highly Charged Ions (HCI)* leads to the loss of electrons from the outer valence shell levels, which are expected to be delocalized over the entire molecular system. Due to the different ionization mechanism, the investigation of the fragmentation of sulfur clusters via HCI collision appears a very interesting pathway to follow (see Chapters 4.1.1 and 4.1.2).
For our investigations we have used ion beams provided by the electron cyclotron resonance

(ECR) source at the Kernfysisch Versneller Instituut (KVI) in Groningen, The Netherlands. The working principle of the HCI source will be briefly presented in Chapter 3.2.2.

In the attempt to improve the understanding of the fragmentation of sulfur clusters, we have also made use of *synchrotron radiation (SR)* from the 3rd generation synchrotron radiation facility BESSY II in Berlin, Germany, in conjunction with a COLTRIMS experimental setup (for details, see Chapter 4.1.3). Experiments on selenium clusters have also been performed (as it will be shown in Chapter 4.2) in which the fragmentation of Se 2p-excited aggregates has been investigated. A brief overview of the operation principle of the synchrotron radiation source will be given in Chapter 3.2.3.

3.2.1 Helium I Discharge Lamp

Small size microwave-induced (2450 MHz) discharge lamps [68] are an established light source when a low power atomic emission line is desired.
Among the advantages of discharge lamps it is worth mentioning the little electrical interference they produce, as well as the compact size of the light source. Also, there is no need for the use of internal electrodes which leads to a discharge environment freer of contamination and less subjected to damage [68]. Another advantage of these light sources is the flexibility in the wavelength, as, in order to change the energy of the radiation one has only to change the gas of the discharge. Thus, typical gases used in microwave driven discharge lamps are He (in order to obtain $h\nu$ = 21.22 eV (He I) or $h\nu$ = 40.78 eV (He II [69]) radiation), N_2, H_2, Ar [68], O_2, CO_2, N_2O or NO_2 [70].

The disadvantages of using a microwave-driven discharge lamp is the fact that the discharge extends over a region of approximately 5 cm as well as that the discharge produces high densities of electrons [71].

In our experiments we have used He as the gas in our Fehsenfeld-type [68] discharge lamp in order to obtain the radiation with $h\nu$ = 21.22 eV. A schematics of the He I discharge lamp used is presented in Fig. 3.3.

The working principle of the microwave-induced discharge lamp is rather simple. The microwave generator is coupled to the discharge cavity via a microwave wave guide. The discharge cavity has the role of transferring energy from the microwave to the gas in the glass capillary (6 mm outer diameter, 1 mm inner diameter). The reflected power from the cavity will exhibit a minimum, and thus the transmitted power to the gas has a maximum, when the resonant frequency of the microwave source is tuned to the one of the cavity and when the two are matched in impedance.

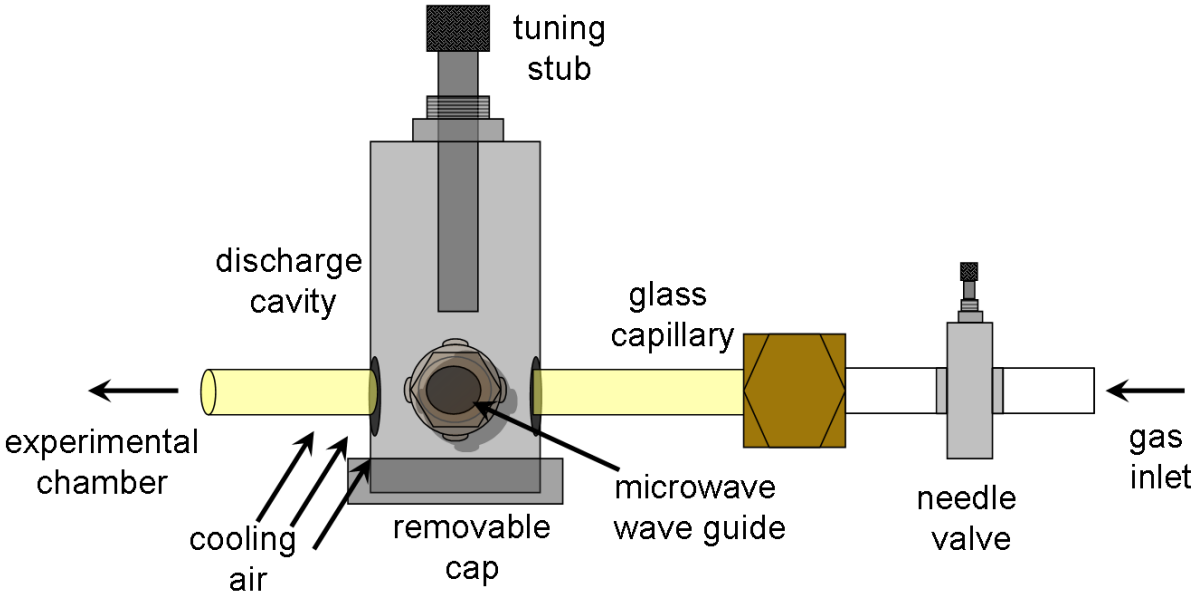

Fig. 3.3: Schematics of He (I) discharge lamp

The adjustment of the minimum reflected power was done with the help of the tuning stub of the discharge cavity (see Fig. 3.3), while the needle valve is used to tune the gas flow through the glass capillary. However, on most cases it is necessary that one initiates the discharge by means of a sparker close to the discharge cavity.

In order to prevent the glass capillary from being overheated and break, cooling air needs to be directed towards the cavity region of the tube. The role of the removable cap of the discharge cavity is to allow for an easier positioning of the discharge tube without breaking the vacuum system.

3.2.2 Highly Charged Ion Beams

The experiments with *Highly Charged Ion (HCI)* beams, were performed at the Kernfysisch Versneller Instituut (KVI) in Groningen (The Netherlands). The ion source is an electron cyclotron resonance (*ECR*) source of the MINIMAFIOS type [72, 73]. Figure 3.4 presents a schematics of the ECR ion source and a brief description will be given in the following (for a more elaborate description see [74]).

In principle, the plasma chamber (1) is floated via the inlet (2) with the desired gas. The multiply charged ions are produced by successive ionization via electron impact. One of the particularities of the MINIMAFIOS type ion sources is that the electrons for the ionization are extracted from a

plasma, and not from a cathode [75].
The plasma is confined in the plasma chamber by a superposition of the magnetic fields created by the permanent hexapole magnet (3) and the electromagnets (4). It is well known that electrons gyrate around magnetic field lines with the cyclotron frequency $\omega_{cyclotron} = \frac{eB}{m_e}$, with B being the magnetic field and e and m_e the charge and mass of the electron, respectively. If, via the microwave cavity (5) we inject microwave radiation with a frequency equal to $\omega_{cyclotron}$ in the confinement region, the electrons will be resonantly accelerated or decelerated, depending on their phase.
The multiply charged ions formed are then extracted from the plasma chamber by using a puller (6) which can negatively biased for efficiency. Since the ion source can be floated on potentials up to 25.000 V, the kinetic energies of the ions obtained can reach $(25.000 \times q)$ eV, where q is the charge of the ion.

The desired charge-over-mass ratio q / A is selected via deflection with a 110° magnet. The ion beam is then transported by making use of triplets of quadrupole magnets, being afterwards deflected by a 45° magnet in the direction of the experimental setup. For focusing the ion beams sets of diaphragms are used.
Crucial parameters for optimizing the ion output are the inlet gas pressure, the microwave power injected (typical values are 0.1 - 0.5 kW) and the current in the electromagnets (usually between 700 - 1000 A).

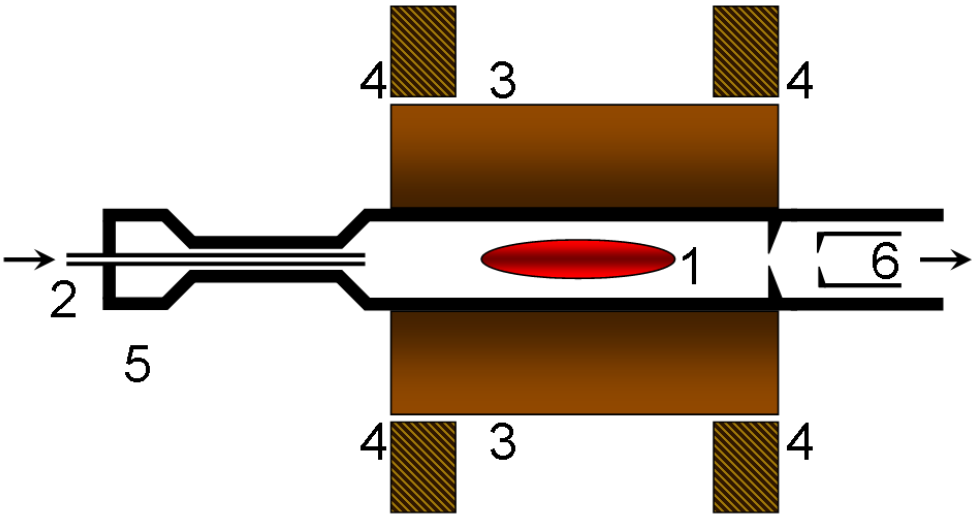

Fig. 3.4: Schematics of the ECR ion source at the KVI Groningen, The Netherlands

3.2.3 Synchrotron Radiation

It is well known the fact that a charged particle in an accelerated motion will emit electromagnetic radiation. *Synchrotron radiation (SR)* occurs when an electron moves at velocities close to the speed of light on a curved trajectory [76, 77].

Figure 3.5 presents a schematics of the storage ring located at BESSY II in Berlin, Germany. Since synchrotron radiation sources are being used since the 1960's, BESSY II itself being operative since 1998, it is considered that a detailed description is not needed, but a rather brief outline of the working principle will suffice (for more insight on synchrotron light source operation see [78] whereas a more detailed description of BESSY II is given in, for example [79] and [80]).

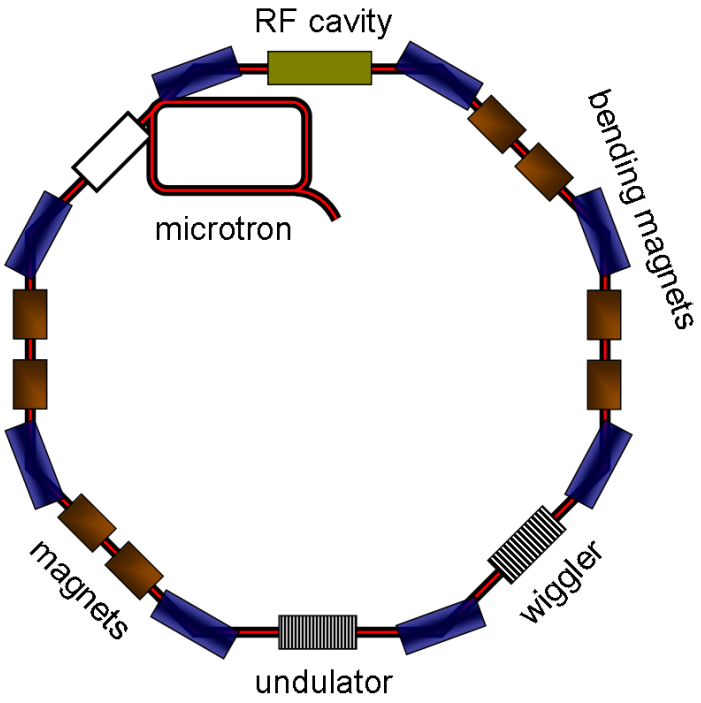

Fig. 3.5: Schematics of an electron storage ring

The electrons produced by an incandescent cathode are accelerated at approximately 100 keV before entering a high frequency linear accelerator, the mycrotron. In the mycrotron, through increasingly strong electromagnetic fields, the electrons are accelerated up to 1.7 GeV. When the electrons reach this energy, through the injection system, they are injected in the storage ring, kept at a typical pressure of 10^{-10} mbar. The electrons are injected in the storage ring in packages (*bunches*) of typically 20 ps length. The typical operating mode of BESSY II is the *multi-bunch mode*, meaning that during an injection more than just one (usually 360 to 400)

"package" of electrons are introduced in the storage ring for orbiting. However, BESSY II can also be operated in the *single-bunch mode*, case in which the electron package orbits the storage ring with a frequency of roughly 1.25 MHz.

The role of the bending magnets (see Fig. 3.5) is to confine the electrons as close as possible to the ideal design orbit, in order to keep the electrons for orbiting for long periods of time. Thus, operating intervals between injections of circa 8 hours and 4 hours are obtained for the multi-bunch and the single-bunch modes, respectively.
Since at the bending magnets the electrons change their direction of movement, synchrotron radiation is emitted.
To make up for the energy lost during each revolution, the electrons pass during their orbiting through a *radio frequency (RF) cavity* where energy is pumped back into the system.

Apart from the bending magnets, in order to harvest synchrotron radiation also from the straight segments of the storage ring, *undulators* and *wigglers* (see Fig. 3.5) are used. These devices consist both of arrays of permanent magnets arranged such that the electrons follow a sinusoidal trajectory, thus leading to the emission of synchrotron radiation.

One of the major differences between undulators and wigglers is that the undulators are typically used to generate radiation with an energy situated in the 50 to 1500 eV interval, while the wigglers are more efficient above 2 keV. The reason for the different spectral region is that the wigglers use far stronger magnetic fields and thus, the deviation of the electrons from their trajectories is more dramatic than in the case of the undulators.

Due to the smaller emission angle with respect to the axis of the undulator, the radiation produced in an undulator can interfere constructively, leading to sharp interference maxima of the harmonics. By contrast, the wiggler spectral interval does not present these maxima, as the radiation does not interfere, due to being emitted at larger angles. It is important to mention that the position of the interference maxima in the undulator spectral interval can be modified by changing the magnitude of the applied magnetic fields, which is done in practice by altering the gap between the arrays of magnets. In order to allow the performance of high resolution spectroscopy the synchrotron radiation is monochromatized before being delivered to the end users.

During the BESSY II experiments described in this thesis, synchrotron radiation from the *PGM 1* beam line set on the *U49/2* (84 periods, 49 mm period length) was used. The U49/2-PGM 1 beam line allows the usage of synchrotron radiation in the energy interval between 70 and 1600 eV, permitting spectroscopic investigations with very high flux with high brilliance on the sample. At the same time, measurements at this beam line can also be performed with high spectral resolution and in constant energy-resolution mode [81, 82].

The optical layout as well as the distances between the elements of the beam line are presented in Fig. 3.6 as reported by Sawhney *et al.* [82]. The optical layout of the monochromator is based

on the design proposed by Lama *et al.* [83].

The incident light on the monochromator is collimated horizontally and vertically by the toroidal gold-coated mirror M_1, being afterwards deflected by M_2 (platinum-coated plane mirror) and diffracted by the grating G. The spherical grating G can be chosen between three gold-coated gratings: a 600 lines/mm one and two 1200 lines/mm ones. After the grating, the gold coated mirror M_3 focused the light on the exit slit. After exiting the monochromator M_4 (plane elliptical gold-coated mirror) focuses the radiation on the experimental sample on a 70 $\mu m \times 20\ \mu m$ area (vertical × horizontal, FWHM[1]).

We have performed measurements in the (150, 230) eV and (1400, 1500) eV energy intervals. In coupled undulator-monochromator mode, for the two energy interval the photon flux stays almost constant at 3×10^{13}photons/s and 10^{10} photons/s respectively, as measured with a fixed exit slit of 150 μm while the resolving power is constant $\frac{E}{\Delta E} > 10000$ [84].

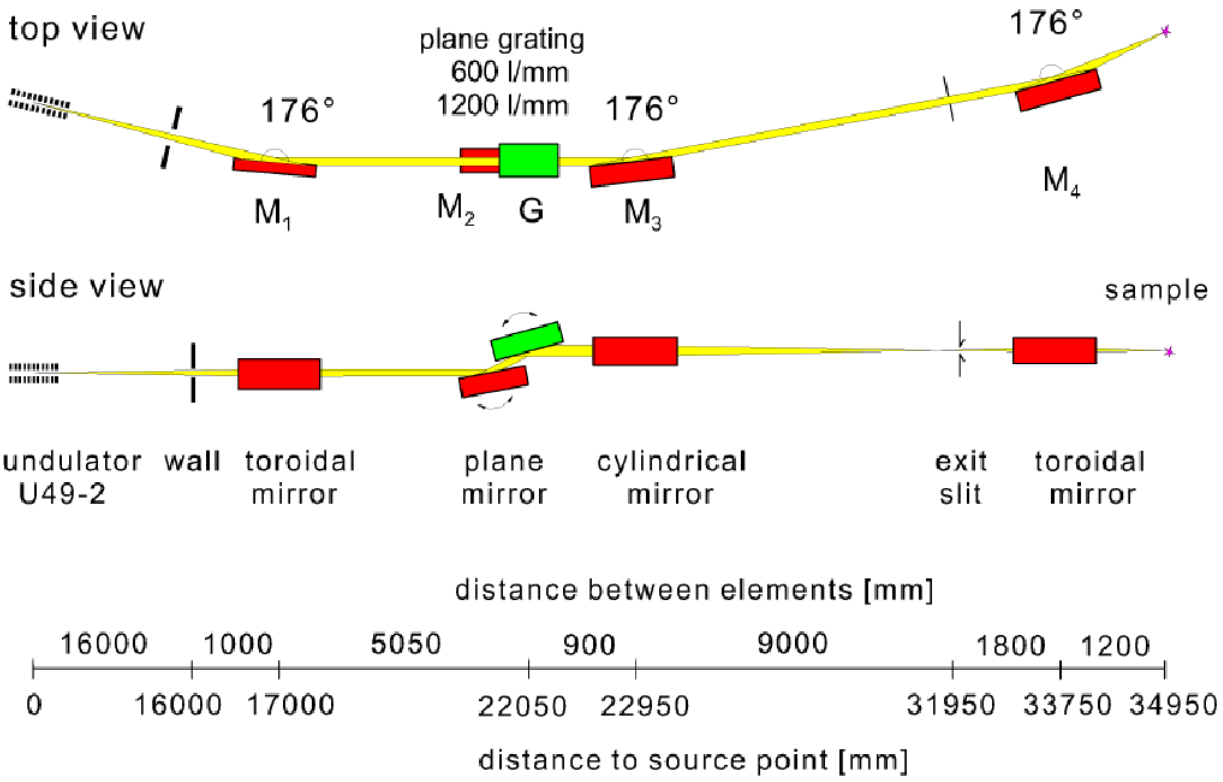

Fig. 3.6: Optical layout of the BESSY U49/2-PGM 1 beam line [82]

[1]Full Width Half Maximum

3.3 The Detectors and The Spectrometers

As the experiments presented in this thesis are based on the detection of single charges, the use of amplification means is necessary. A convenient way to amplify the signal obtained from single particles is to use as detection devices micro-channel plate (MCP) detectors.

The micro-channel plate detector consists of an array of very fine tubes (micro-channels) [85] made from a highly resistive material with diameters of 10 μm and lengths of 1 mm, (see Fig. 3.7a.), oriented at an angle of 8 degrees with respect to the normal to the MCP front plane [86].

The particles hitting the MCP detector lead to the emission of secondary electrons in the micro-channels, which are accelerated towards the back of the MCP by applying a voltage on the front and on the back of the channel plates. For the experiments we performed we typically applied ≈ -2350 V on the front MCP and ≈ -150 V on the back of the MCP stack. As the accelerated electrons collide with the walls of the micro-channels they produce avalanches of secondary electrons, yielding an amplification factor per MCP of typically 10^3 to 10^4.

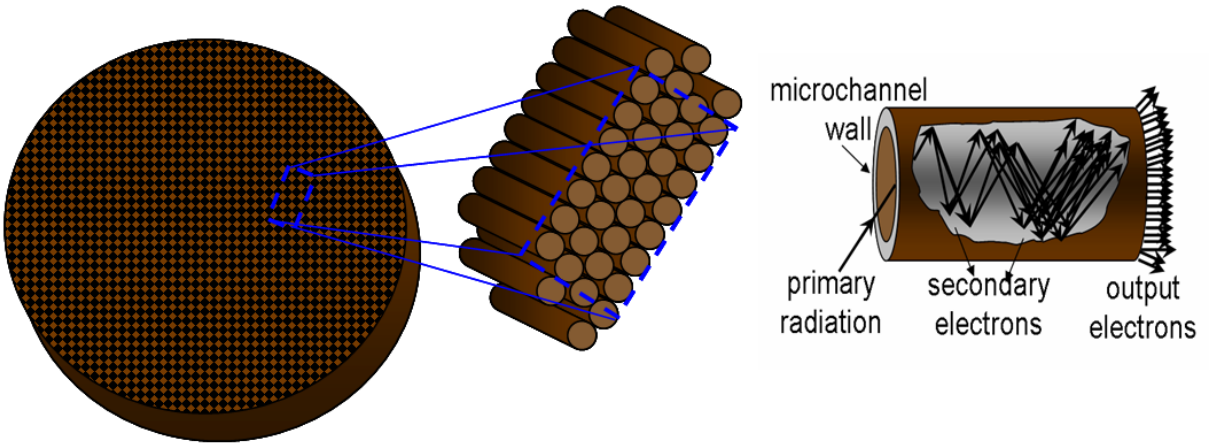

Fig. 3.7: Schematics of a micro-channel plate detector

In order to improve the amplification factor of the detector it is common to use a stack of two multi-channel plate disposed in a so called "Chevron geometry", meaning that the two plates are oriented such that any possible positive ion production at the output of the second plate is inhibited [85]. With such a configuration an amplification of 10^6 to 10^7 is normally achieved.

In order to collect the signal amplified by the multi-channel plate detector for further analysis, behind the MCP detectors an anode is to be found. Depending on the experimental setup used, for the experiments performed the anode consisted in a 2 mm thick copper plate (in the Wiley-McLaren type time of flight mass spectrometer) or a delay line anode (in the COLTRIMS spectrometer).

3.3.1 The Time-of-Flight Mass Spectrometer

The majority of the experiments were performed by making use of a Wiley-McLaren type time of flight mass spectrometer [59]. A schematics of such a mass spectrometer is presented in Fig. 3.8, and the working principle will be described in short in the following.

Briefly, the spectrometer consists of three regions: the extraction region (E), the acceleration region (A) and the drift region (D). After the ions have passed the three regions they are collected on an MCP detector, and the resulting signal is collected from the copper anode behind the channel-plates for further processing.

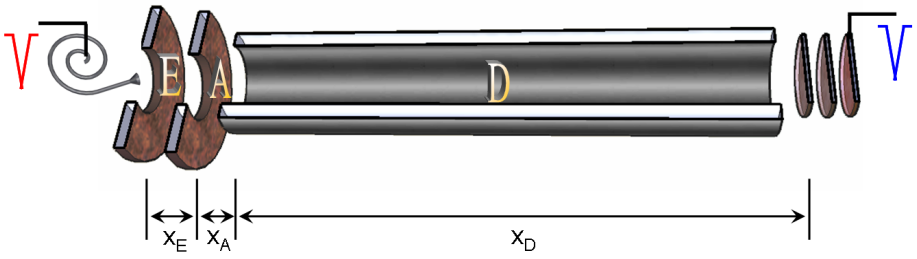

Fig. 3.8: Schematics of a Wiley-McLaren type time of flight mass spectrometer

In the middle of the extraction region of the spectrometer (with $x_E = 10$ mm) the cluster beam is crossed by the ionizing beam (synchrotron radiation, highly charged ion beam, He (I) radiation). This results in the excitation of the clusters and the release of one or more electrons. In order to extract the ions and the electrons from the E region, an electric field $\overrightarrow{E_E}$ is applied. For the experiments of the present work $\overrightarrow{E_E} = 310$ V/cm. Thus, the ions are extracted from the E region in the direction of region A, whereas the electrons are pushed in the opposite direction. For experiments where also the recording of the electrons is desired (for instance, a coincidence experiment), an electron detector (such as a stack of MCP's or a channeltron[2]) can also be mounted on the spectrometer, opposite to the ion detector.

The A region had in the spectrometer used a length of $x_A = 10$ mm. This region has the role of accelerating the ions towards the detector via an electric field $E_A \approx 1200$ V/cm.

The D region of the spectrometer had a length of 390 mm and is an electric field free region ($E_D = 0$ V/cm). This region of the spectrometer serves to improve the time resolution and the space focusing of the ions [59]. By space focusing it is understood that each ion formed in the E region will leave region A with a velocity dependent on its initial position and its m/q ratio, where

[2] a single channel electron multiplier

m and q denote the mass and the charge, respectively, of the ion, such that different ions with the same m/q ratio will arrive at the detector at the same time.

Thus, when the space focusing condition is fulfilled, we can write the total flight time (t) of an ion in the spectrometer as being:

$$t = t_E + t_A + t_D \tag{3.1}$$

with t_E, t_A and t_D being the flight times corresponding to regions E, A and D respectively, and having the magnitudes defined by:

$$t_E = 1.02\frac{\sqrt{2m}}{qE_E}(\sqrt{U_0 + qx_E E_E} \pm \sqrt{U_0})$$

$$t_A = 1.02\frac{\sqrt{2m}}{qE_A}(\sqrt{U} - \sqrt{U_0 + qx_E E_E}) \tag{3.2}$$

$$t_D = 1.02\sqrt{2m}\frac{x_D}{2\sqrt{U}}$$

where the "-" and the "+" signs indicate that the initial velocity is directed towards and away from the detector, respectively, and U_0 and U are the kinetic energies of the ion in the initial moment and when it leaves region A.

As the times of flight of the ions in the spectrometer depend linearly on the square-root of the m/q ratio, we can write:

$$t = a\sqrt{\frac{m}{q}} + b \tag{3.3}$$

where a and b are constants. From Eq. 3.3 we can deduce that for two ions of masses m_1 and m_2:

$$\frac{t_1}{t_2} = \sqrt{\frac{m_1}{m_2}} \tag{3.4}$$

where t_1 and t_2 are the flight times of the two ions, respectively. Combining Eq. 3.3 and 3.4 one can determine the constant values a and b, and use the result for calibration purposes.

3.3.2 The COLTRIMS Reaction Microscope

The term "COLTRIMS" is an acronym and stands for COLd - Target - Recoil - Ion - Momentum - Spectroscopy [87, 88, 89]. This is a momentum space imaging technique used for the investigation of the dynamics of the ionization and fragmentation reactions of atoms, molecules and clusters.The technique makes use of the large area position- and time-sensitive multi-hit electron and ion detectors developed in the last two decades, and it was used for the first time in the late 80's [90, 91, 92].

The main advantage of the technique over other fragmentation investigation techniques is that it provides a 'kinematically complete' picture of the reaction. By 'kinematically complete' it is understood that the momenta of all the involved particles are derived, but the spin of the particles is not determined, as so far there are no efficient spin-sensitive electron detectors.

Another major advantage of using the COLTRIMS system is that the technique allows for detecting the particles resulting from a fragmentation process with a detection solid angle of 4π with a very high accuracy. There have been reports of energy resolutions of below 1 meV for slow electrons, while ion momenta have been reported with a resolution of up to 1 μeV [93, 94, 95, 96].

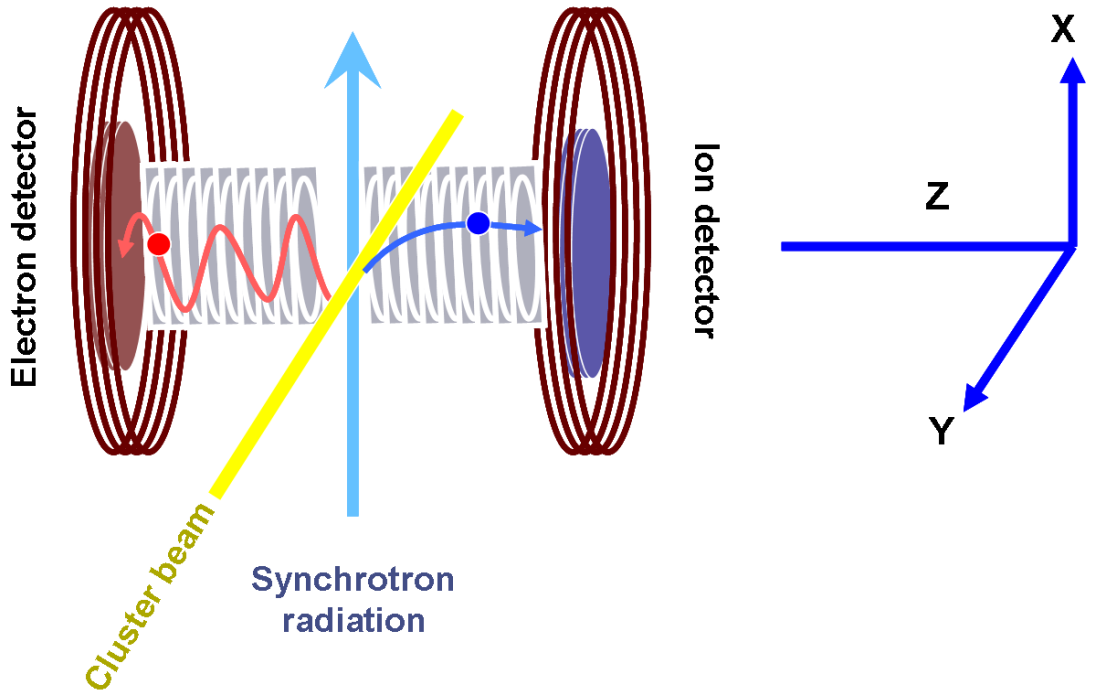

Fig. 3.9: Schematics of the working principle of a COLTRIMS experimental setup

The principle of the technique is based on combining the measuring of the time of flight of the emerging fragments with a position sensitive detector which is also capable of accepting multiple hits within few ns [97, 98].

The spectrometer depicted in Fig. 3.9 shows a schematics of the one that was used in our experiments.

The positive ions are extracted perpendicular to the plane defined by the transversal section through the spectrometer which contains the direction of the ionizing synchrotron radiation, while the electrons are pushed in the exactly opposite direction.
The cations are accelerated over a distance $x_A^i = 22$ mm (see also Fig. 3.10) by a weak homogeneous static electric field ($E = 6\ V/cm$). No drift region is used for the ion branch of the spectrometer [99, 100, 101].

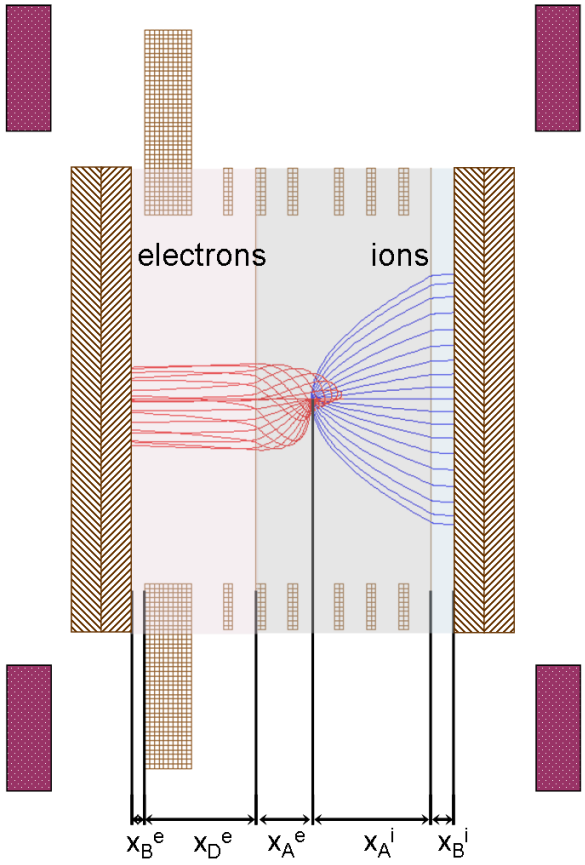

Fig. 3.10: Trajectories of electrons and ions in the COLTRIMS spectrometer

After passing a woven grid they are accelerated over a so called "booster region" (region x_B^i in Fig. 3.10) over 2380 V onto a micro-channel plate detector. The "booster region" has only the role of

transporting the ions to the detector and it does not influence the projections of the initial kinetic momenta on the three axes of the spectrometer (x, y and z, where x and y define the position and z defines the flight time of the ions)

The electron part of the spectrometer is built following strictly the Wiley-McLaren [59] time focusing condition. This means that the electrons are accelerated over a distance $x_A^e = 13$ mm (see also Fig. 3.10) and then they enter a field free drift region $x_D^e = 26$ mm. The exact ratio of 1 to 2 between the length of acceleration and drift region assures that electrons starting at slightly different positions along the electric field lines arrive at the same time at the detector.
In order to ensure the confinement of the electrons in the spectrometer for kinetic energies of the order of few tenths of eV, a magnetic field is needed (in our case, we used a magnetic field of 10 Gauss). However, for electrons with kinetic energies exceeding 30 eV the magnetic field guiding them on helical trajectories fails to confine them within the detectable region for all emission angles.
After exiting the field-free region, the electrons pass trough a "booster region" (x_B^e) (see Fig. 3.10) where they are accelerated over 2600 V before hitting the channel-plate detector.

3.3.2.1 The Position Sensitive Detector

In order to achieve the kinematically complete picture of a fragmentation process, one needs to determine, as mentioned in the previous section, the kinetic momenta of all the involved particles. This means that one needs to determine the time of flight as well as the impact position of single particles on the detector. In order to be able to observe single particles, our detector consists of a micro-channel plate detector behind which a delay-line position sensitive anode commercially available from the Roentdek company [102] is to be found.

The electrons formed through secondary emission in the micro-channels are accelerated after the output from the MCP towards the delay line anode by applying a voltage of about $300 - 500$ V on the anode.
The delay line anode consists of two (a quadratic anode) or three (a hexagonal anode) pairs of thin copper wires (50 μm in diameter) which are disposed at 90° (60°, respectively) with respect to one another (see Fig. 3.11). The advantage of the third pair of wires is a better time (up to $\approx$ 500 ps) and position resolution ($<$ 200 μm) [103].

Figure 3.11 presents a schematics of a quadratic and a hexagonal delay line anode, as well as a side view of a delay line anode. The schematically drawn wires as well as the distances between them are not scaled, but rather depicted such that they provide more clarity in the description.

Each one of the two (three, respectively) layers consists of a pair of wires that are tightly wound such that the distance between two adjacent wires is 0.5 mm and that a gap of approximately 1 mm is left between the different layers. By setting the voltage on one of the wires (from here on

referred to as "the signal wire") in a pair to a slightly higher voltage (30 – 50 V) than the other one (henceforth addressed to as "the reference wire") one ensures that the electrons are collected on the signal wire only [97].

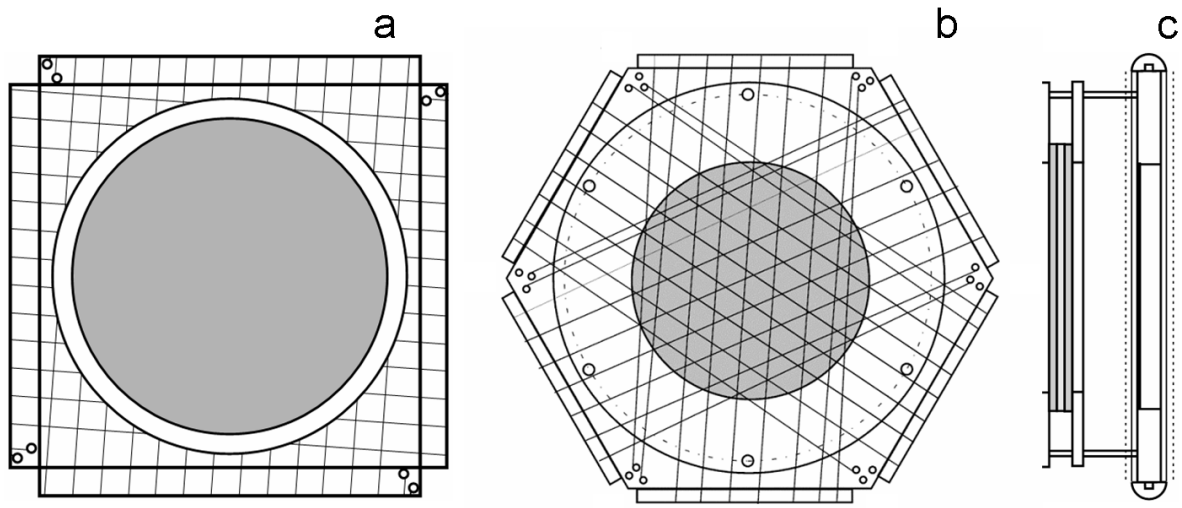

Fig. 3.11: Schematics of a quadratic (a), hexagonal (b) and side view (c) of a delay line anode [97]

Upon hitting the anode, the electron cloud will induce a signal in the wire, which will propagate towards both ends of the wire (see Fig. 3.12 for a schematics of the principle [104]) where it is picked up for further processing.

From determining the difference in the propagation time of the signal to both of the ends of the wires one can derive the position (X, Y) where the signal was picked up, as described by (for a quadratic delay line anode):

$$X = (x_1 - x_2) \times v_\perp$$
$$Y = (y_1 - y_2) \times v_\perp \tag{3.5}$$

where x_1, x_2, y_1, y_2 represent the measured signal arriving times of the signals to the four ends of the of the delay lines. As a start signal for determining the four arrival times, one can use either the signal from the front or from the back of the MCP stack. In Eq. 3.5, $v_\perp$ stands for the transverse propagation velocity of the signal on the delay line anode, and is typically of the order of 1 mm/s. The time sums $x_1 + x_2$ and $y_1 + y_2$ are constant and irrespective of the hit position and can be used as a time of flight mark if the start signal corresponds to an external trigger (a laser pulse or a synchrotron bunch marker). The time sums also allow for consistency checks of the validity of the recorded position information [104].

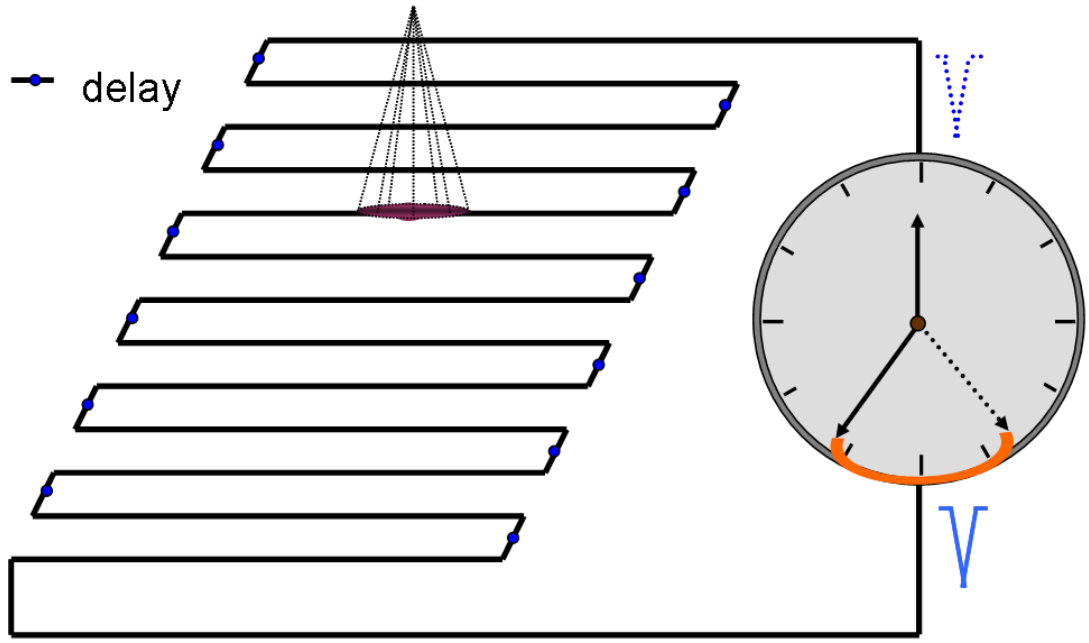

Fig. 3.12: Schematics of the delay line principle

However, for a hexagonal delay line anode, when determining the position (X, Y) of the hit one must take into account the fact that the three layers (*u, v, w*) are positioned with a angle of 60° to each other [105]. Therefore, Eq. 3.5 will be written:

$$\begin{aligned} u &= c_u(t_{u1} - t_{u2}) \\ v &= c_v(t_{v1} - t_{v2}) \\ w &= c_w(t_{w1} - t_{w2}) \\ X &= u \\ Y &= \frac{1}{\sqrt{3}}(2w - u) \end{aligned} \tag{3.6}$$

for a hexagonal anode, where c_u, c_v and c_w respectively are conversion factors from the position of the hit on the anode in ns into the position in mm for the three layers. Since for any two of the three layers the recorded information is linearly independent, we can use any combination of two layers to determine the (X, Y) position of the hit, namely:

$$X = v + w$$
$$Y = \frac{1}{\sqrt{3}}(w - u) \tag{3.7}$$

or

$$X = u$$
$$Y = \frac{1}{\sqrt{3}}(u - 2v) \tag{3.8}$$

Further on, the information extracted about the time of flight of the particles and the hit position on the anode can be used to determine the trajectories of the particles as well as the initial kinetic momenta of the particles. This information can also be used for reconstructing the position of the center of mass of the particles at the time of the dissociation.
Thus, one obtains for the three projections on the x, y and z axes (p_{ex}, p_{ey} and p_{ez}) of the initial kinetic momenta $\overrightarrow{p_e} = m_e\overrightarrow{v_e}$ of the electrons the following equations [106, 107] :

$$p_{ex} = m_e\frac{-x_e a - by_e}{a^2 + b^2}$$
$$p_{ey} = m_e\frac{-x_e b - ay_e}{a^2 + b^2} \tag{3.9}$$
$$p_{ez} = m_e\frac{x_A^e}{t_e} - \frac{q_e E_z}{2}t_e$$

where m_e is the rest mass of the electron, x_e and y_e are the hit position of the electron on the detector, t_e is the flight time of the electron, x_A^e is the acceleration distance of the electron in the spectrometer (see Fig. 3.10), E_z is the z component of the electric field in the spectrometer and

$$a = \frac{1 - \cos\omega t_e}{\omega}$$

and

$$b = \frac{\sin\omega t_e}{\omega}$$

with $\omega = \frac{e}{m_e}B$ being the cyclotron frequency of the electron in the applied magnetic field $\overrightarrow{B}$.

Therefore, the equations describing the trajectory of the electron in the spectrometer will be written:

$$x_{e,initial}(t) = \frac{v_{ey}}{\omega}(1 - \cos\omega t) + \frac{v_{ex}}{\omega}\sin\omega t$$

$$y_{e,initial}(t) = \frac{v_{ex}}{\omega}(\cos\omega t - 1) + \frac{v_{ey}}{\omega}\sin\omega t \tag{3.10}$$

$$z_{e,initial}(t) = \frac{e}{2m_e}E_z t^2 + v_{ez}t$$

where v_{ex}, v_{ey} and v_{ez} are the respective projections on the three axes of the velocity of the electron.

For the recorded ions, the determination of the initial kinetic momenta is easier to achieve as compared to the electrons case, as the ion arm of the spectrometer does not obey the Wiley-McLaren [59] focusing condition. Therefore, one can derive the projections of the initial kinetic momentum $\overrightarrow{p_i} = m\overrightarrow{v_i}$ on the three axes (p_{ix}, p_{iy} and p_{iz}) as follows [99]:

$$p_{ix} = \frac{m_i(x_i - x_{i,initial})}{t_i}$$

$$p_{iy} = \frac{m_i(y_i - y_{i,initial})}{t_i} - v_{cluster}m_i \tag{3.11}$$

$$p_{iz} = \frac{m_i z_{i,initial}}{t_i} - \frac{F_r q_i t_i}{2}$$

where $z_{i,initial} = x_A^i + x_B^i$ with x_A^i and x_B^i as depicted in Fig. 3.10, m_i refers to the mass of the ion, $v_{cluster}$ stands for the velocity of the cluster beam and F_r is the force acting on the ion of charge q_i in the spectrometer. x_i and y_i define the position where the ion hits the ion detector, while $x_{i,initial}$, $y_{i,initial}$ and $z_{i,initial}$ define the position of the starting point of the trajectory with t_i standing for the flight time of the ion.

It is, however, important to point out that the coordinates of the starting point of the trajectory ($x_{i,initial}$, $y_{i,initial}$ and $z_{i,initial}$) suffer from the uncertainty introduced by the dimension of the interaction region between the cluster beam and the focus of the synchrotron radiation beam. Therefore, the size of the interaction volume is generally the limiting factor in momentum resolution and thus in energy resolution [99, 108]

However, in order to improve the resolution of the spectrometer, one can determine the relative kinetic momenta ($\overrightarrow{p_{rel}}$) of the ions with respect to each other, rather than the kinetic momenta of the individual ions [99].

For a two body break up mechanism, one can write $\overrightarrow{p_{rel}}$ as follows:

$$\overrightarrow{p_{rel}} = \overrightarrow{p_1} = -\overrightarrow{p_2} \tag{3.12}$$

which will lead to

$$p_{rel,ix} = m_1 m_2 \frac{x_1 - x_2}{t_2 m_1 + t_1 m_2}$$

$$p_{rel,iy} = m_1 m_2 \frac{(y_1 - y_2) + v_{cluster}(t_2 - t_1)}{t_2 m_1 + t_1 m_2} \tag{3.13}$$

$$p_{rel,iz} = \frac{E}{2}\left(\frac{{t_2}^2 q_2 m_1 - {t_1}^2 q_1 m_2}{t_1 m_2 + t_2 m_1}\right)$$

where t_1, t_2, m_1, m_2, q_1 and q_2 stand respectively for the flight time, the masses and the charges of the two fragments. As one can note, Eqs. 3.13 no longer depend on the initial position of parent ion ($x_{i,initial}$, $y_{i,initial}$ and $z_{i,initial}$) but are a function of the hit position on the detector, $(x_1 - x_2)$ and $(y_1 - y_2)$.

We can further on use the relative kinetic momentum obtained for the calculation of the kinetic energy release of the dissociation given by:

$$KER = \frac{p_{rel}^2}{2\mu_{1,2}} = \frac{p_{rel,ix}^2 + p_{rel,iy}^2 + p_{rel,iz}^2}{2\mu_{1,2}} \tag{3.14}$$

with $\mu_{1,2}$ being the reduced mass of the system composed of the two ions, defined by:

$$\mu_{1,2} = \frac{m_1 m_2}{m_1 + m_2} \tag{3.15}$$

Combining Eqs. 3.9 with eq. 3.12 and 3.13, one can derive the initial place where the reaction took place, namely:

$$x_{initial} = \frac{t_2 m_1 x_1 + t_1 m_2 x_2}{t_1 m_2 + t_2 m_1}$$

$$y_{initial} = \frac{t_2 m_1 y_1 + t_1 m_2 y_2}{t_1 m_2 + t_2 m_1} \tag{3.16}$$

An calculation of the z position of the reaction place would be superfluous, as the electron branch of the spectrometer is built, as mentioned in the previous section, in strict respect to the Wiley-McLaren time focusing condition [59]. By determining the initial position of the parent ion one can improve the resolution of the determined kinetic momenta of the ions. The initial position of

the ions can also serve as an efficient gate for reducing the background noise and for eliminating false coincidence signals.

Using Eq. 3.13 and taking into account kinetic momentum conservation, one can derive the flight time of the second ion, t_2 as a function of the arrival time of the first ion, t_1 as being:

$$t_2 = \frac{(x_A^i + x_B^i)m_1}{q_2 E_1 t_1} - \frac{q_1 t_1}{2q_2} + \sqrt{\frac{2(x_A^i + x_B^i)m_2}{q_2 E_1} + (\frac{(x_A^i + x_B^i)m_1}{q_2 E_1 t_1} - \frac{q_1 t_1}{2q_2})^2} \tag{3.17}$$

By setting proper gates on t_2, one has thus the possibility of selecting, for further examination, one-by-one the coincidence channels from the raw PIPICO spectrum.